The Astrophysical Journal, 719:1619–1632, 2010 August 20 doi:10.1088/0004-637X/719/2/1619

HUBBLE SPACE TELESCOPE FAR-ULTRAVIOLET OBSERVATIONS OF BRIGHTEST CLUSTER GALAXIES: THE ROLE OF STAR FORMATION IN COOLING FLOWS AND BCG EVOLUTION

Kieran P. O'Dea[1,5], Alice C. Quillen[1], Christopher P. O'Dea[2], Grant R. Tremblay[2], Bradford T. Snios[2], Stefi A. Baum[2], Kevin Christiansen[2], Jacob Noel-Storr[2], Alastair C. Edge[3], Megan Donahue[4], and G. Mark Voit[4]
[1] Department of Physics and Astronomy, University of Rochester, Rochester, NY 14627, USA
[2] Rochester Institute of Technology, 84 Lomb Memorial Drive, Rochester, NY 14623, USA
[3] Department of Physics, Institute for Computational Cosmology, Durham University, Durham DH1 3LE, UK
[4] Physics and Astronomy Department, Michigan State University, East Lansing, MI 48824, USA
Received 2010 March 30; accepted 2010 June 16; published 2010 August 2

ABSTRACT

Quillen et al. and O'Dea et al. carried out a *Spitzer* study of a sample of 62 brightest cluster galaxies (BCGs) from the *ROSAT* brightest cluster sample, which were chosen based on their elevated Hα flux. We present *Hubble Space Telescope* Advanced Camera for Surveys far-ultraviolet (FUV) images of the Lyα and continuum emission of the luminous emission-line nebulae in seven BCGs found to have an infrared (IR) excess. We confirm that the BCGs are actively forming stars which suggests that the IR excess seen in these BCGs is indeed associated with star formation. Our observations are consistent with a scenario in which gas that cools from the intracluster medium fuels the star formation. The FUV continuum emission extends over a region ~7–28 kpc (largest linear size) and even larger in Lyα. The young stellar population required by the FUV observations would produce a significant fraction of the ionizing photons required to power the emission-line nebulae. Star formation rates estimated from the FUV continuum range from ~3 to ~14 times lower than those estimated from the IR, however, both the Balmer decrements in the central few arcseconds and detection of CO in most of these galaxies imply that there are regions of high extinction that could have absorbed much of the FUV continuum. Analysis of archival Very Large Array observations reveals compact radio sources in all seven BCGs and kpc scale jets in A-1835 and RXJ 2129+00. The four galaxies with archival deep *Chandra* observations exhibit asymmetric X-ray emission, the peaks of which are offset from the center of the BCG by ~10 kpc on average. A low feedback state for the active galactic nucleus could allow increased condensation of the hot gas into the center of the galaxy and the feeding of star formation.

Key words: galaxies: clusters: intracluster medium – galaxies: elliptical and lenticular, cD – galaxies: jets – ultraviolet: galaxies

Online-only material: color figures

1. INTRODUCTION

The assembly of rich, X-ray luminous galaxy clusters is such that the largest baryonic mass fraction of the system is occupied by hot $T \sim 10^7$–10^8 K gas pervading the intracluster medium (ICM). In the central regions ($r \lesssim$ 10–100 kpc) of many clusters, the time scale for this gas to cool to $T \lesssim 10^4$ K can be shorter than the cluster lifetime (e.g., Cowie & Binney 1977; Fabian & Nulsen 1977; Edge et al. 1992), giving rise to a subsonic, pressure-driven cooling flow that deposits mass onto the luminous and massive cD elliptical galaxy at the cluster center. "Cool core" clusters such as these often exhibit intense optical emission-line nebulae associated with these central brightest cluster galaxies (BCGs). The nebulae exhibit extended Lyα emission (Hu 1992) and far-ultraviolet (FUV) continuum emission (O'Dea et al. 2004). A previous study of two BCGs, A1795 and A2597 (O'Dea et al. 2004), found that the nebula exhibited both a diffuse component of Lyα and more compact features such as knots and filaments. The Lyα emission was closely tied to the radio morphology suggesting that star formation and associated ionization were present at the edges of radio lobes. That work demonstrated how Lyα and FUV continuum observations provide unique constraints on the physical properties of the nebulae in clusters. The far-UV continuum together with optical and infrared observations constrain the star formation history and the properties of young stars associated with the nebula. The Lyα to Hα or Hβ flux ratio is a diagnostic of ionization, metal and dust content (Ferland & Osterbrock 1985; Binette et al. 1993).

Previous optical and UV observations have found evidence for significant star formation in some BCGs in cool core clusters (Johnstone & Fabian 1987; Romanishin 1987; McNamara & O'Connell 1989, 1993; McNamara 2004; McNamara et al. 2004; Hu 1992; Crawford & Fabian 1993; Hansen et al. 1995; Allen 1995; Smith et al. 1997; Cardiel et al. 1998; Hutchings & Balogh 2000; Oegerle et al. 2001; Mittaz et al. 2001; O'Dea et al. 2004; Hicks & Mushotzky 2005; Rafferty et al. 2006; Bildfell et al. 2008; Loubser et al. 2009; Pipino et al. 2009). Nearly all BCGs with young stellar populations are in cooling flows (Bildfell et al. 2008; Loubser et al. 2009). However, some BCGs in cooling flows do not have significant star formation (Quillen et al. 2008; Loubser et al. 2009). Hence, BCGs exhibiting elevated rates of star formation could be those experiencing a low level of feedback from the active galactic nucleus (AGN). Evidence for residual cooling can be inferred from the reservoirs of cold gas found in BCGs. Alternatively, star formation could also be attributed to stripping from a gas-rich galaxy (Holtzman et al. 1996). Recent estimates of condensation and star formations rates show that in a few systems they are in near agreement (e.g., O'Dea et al. 2008). Recent work suggests that star formation tends to occur when the central cooling time drops below a critical value (Rafferty et al. 2008; Voit et al. 2008; Cavagnolo et al. 2008). In our study of 62 BCGs with the *Spitzer* IRAC and MIPS we found that about half of the BCGs in our

[5] Also at SUNY Geneseo, 1 College Circle, Geneseo, NY 14454, USA.

sample showed evidence for mid-IR emission produced by star formation (Quillen et al. 2008). The IR emission was typically unresolved by the 8 arcsec (FWHM) point-spread function of MIPS at 24 μm.

In this study, we enlarge the sample of objects studied by O'Dea et al. (2004) to include more distant BCGs and those with higher star formation rates (estimated in the IR). BCGs with high Hα luminosities were chosen from the *ROSAT* brightest cluster sample (BCS; Ebeling et al. 1998). Their Hα luminosities are in the range 10^{42}–10^{43} erg s^{-1}. These galaxies have been observed with the *Spitzer Space Telescope* (Quillen et al. 2008; O'Dea et al. 2008). The FUV *Hubble Space Telescope* (*HST*) observations presented here allow us to confirm that ongoing star formation is present in the BCGs and to determine its spatial scale and morphology (subject to dust extinction). Throughout this paper, we use $H_0 = 71$ km s^{-1} Mpc^{-1}, $\Omega_M = 0.27$, and $\Omega_\Lambda = 0.73$.

2. OBSERVATIONS

2.1. FUV Continuum and Lyα Images

Observations were obtained with the solar blind channel (SBC) MAMA detector of the Advanced Camera for Surveys (ACS; Clampin et al. 2004) on the *HST* during cycle 11 (program 11230, PI: K. P. O'Dea). Each galaxy was observed in two long pass filters, the one containing the Lyα line, the other redward of this line to measure the continuum. The *F140LP* filter containing the Lyα line was used for all galaxies except the nearer BCGs, A11 and A1664, which were observed using the *F125LP* filter. The continuum filter chosen was *F140LP* for objects with redshift $z < 0.11$, *F150LP* for objects with redshift $0.11 < z < 0.19$ (ZWCL8193, A11, and A1664) and the *F165LP* filter for the remaining objects with $0.19 < z < 0.31$ (A1835, ZWCL348, RXJ 2129+00, and ZWCL3146). Observations were obtained using a three point position dither. The exposure time in each filter was 1170 s so that the observations in the two filters were approximately one *HST* orbit per galaxy. Observations were taken between 2008 March and 2009 February. The long pass filters, *F125LP*, *F140LP*, *F150LP*, and *F165LP*, have pivot wavelengths of 1438, 1527, 1611, and 1758 Å, respectively, and similar maximum wavelengths of 2000 Å but minimum or cutoff wavelengths of 1250, 1370, 1470, and 1650 Å, respectively. The pixel scale for the SBC is approximately $0\farcs034 \times 0\farcs030$ pixel^{-1}. The camera field of view is $34\farcs6 \times 30\farcs8$. These FUV observations are summarized in Table 1.

The ACS/SBC images were reduced with the ACS calibration pipeline producing calibrated drizzled images. Continuum images were shifted to the position of the line images and subtracted from the line images after multiplication by an adjusted corrective factor larger than 1 to take into account the additional continuum photons present in the line images. Our procedure was to increase the correction factor until regions of the image became negative. FUV and continuum subtracted Lyα images are shown in Figures 1–7.

2.2. Comparison Images

At the same time optical images were observed with the WPFC2 camera on board *HST* using the broad band *F606W* filter for A1664 and ZWCL 8193. Visible broad band images observed with WFPC2 were available from the Hubble Legacy Archive for the remaining galaxies in either the *F702W* filter (A1835) or the *F606W* filter (ZWCL 348, ZWCL 3146, A11, and RXJ 2129+01). The broad band optical images are shown for comparison in Figures 1–7.

Table 1
HST Observation Log

Source	R.A.	Decl.	z	kpc/″	Line/Cont	Filter
A11	00:12:33.87	−16:28:07.7	0.151	2.60	Line	*F125LP*
					Cont.	*F150LP*
A1664	13:03:42.52	−24:14:43.8	0.128	2.26	Line	*F125LP*
					Cont.	*F150LP*
A1835	14:01:02.10	+02:52:42.8	0.253	3.91	Line	*F140LP*
					Cont.	*F165LP*
ZWCL 348	01:06:49.39	+01:03:22.7	0.254	3.92	Line	*F140LP*
					Cont.	*F165LP*
ZWCL 3146	10:23:39.62	+04:11:10.8	0.290	4.32	Line	*F140LP*
					Cont.	*F165LP*
ZWCL 8193	17:17:19.21	+42:26:59.9	0.175	2.94	Line	*F140LP*
					Cont.	*F150LP*
RXJ 2129+00	21:29:39.96	+00:05:21.2	0.235	3.70	Line	*F140LP*
					Cont.	*F165LP*

Notes. *HST* observations obtained under program 11230 (PI: K. P. O'Dea). The exposure time in each long pass filter was 1170 s. Positions are given in degrees for epoch J2000 and are measured from radio source positions in archival VLA data at 8.5 or 5 GHz. See Table 2 for a summary of the archival radio images.

We have overlaid 3 μm continuum observations as contours in Figures 1–7 on the FUV continuum images. These images were taken with the IRAC camera on the *Spitzer Space Telescope* and are described by Egami et al. (2006) and Quillen et al. (2008). We find that the FUV and Lyα emission are located near the center of the BCGs as seen at 3 μm.

Chandra X-ray Observatory observations with the Advanced CCD Imaging Spectrometer (ACIS) were available from the archive for four of the galaxies: A1664, A1835, ZWCL 3146, and RXJ 2129+00. Exposure times were 11, 22, 49, and 12 ks, respectively. The event files were binned to 1″ pixels and the resulting images smoothed with the *ciao* adaptive smoothing routine *csmooth* using the algorithm by Ebeling et al. (2006). Constant surface brightness X-ray contours are shown for these four galaxies in Figures 2, 3, 5, and 7 overlaid on the continuum subtracted Lyα images.

Where available, we selected high resolution Very Large Array (VLA) observations from the NRAO archive. For some sources we chose an additional data set in order to obtain a complementary lower resolution image. The NRAO AIPS package was used for the calibration, imaging, self-calibration, and deconvolution. The properties of the final images are given in Table 2. We detected a faint point source in all the BCGs. The flux densities of the point sources are given in Table 4. These high resolution observations are not sensitive to very diffuse emission.

Figures 1–7 have been centered at the location of the central radio sources as measured from VLA archival data at 5 or 8.5 GHz (with positions listed in Table 4). Coordinate errors measured from *HST*, *Spitzer Space Telescope*, and ACIS *Chandra X-ray Observatory* observations are of order an arcsecond. The FUV and Lyα images lack point sources that could be used to register the images at sub-arcsecond scales.

3. RESULTS

3.1. UV Morphology

We find that all seven galaxies observed display extended emission in both FUV continuum and Lyα emission. The FUV

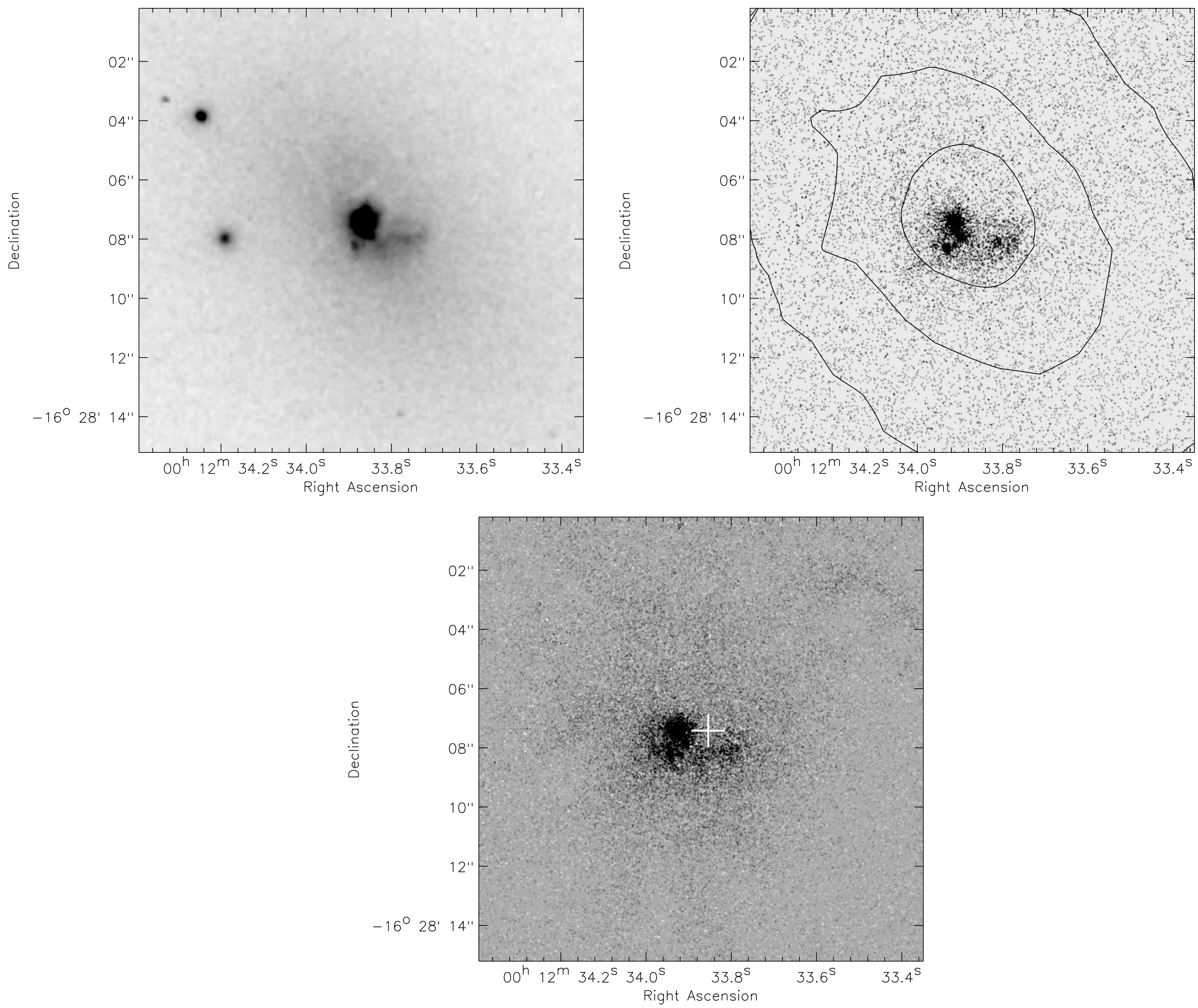

Figure 1. A11. Upper left: *HST* WFPC2 *F606W* optical image. Note the dust lane. Upper right: *HST* SBC FUV continuum image with 3 μm *Spitzer* IRAC band 1 contours overlaid. Contour separation is a factor of two in surface brightness. Bottom: continuum subtracted *HST* SBC Lyα image of A11. The white cross marks the position of the unresolved VLA radio source (Table 4). At the redshift of A11 ($z = 0.151$), 1″ corresponds ∼2.6 kpc.

Table 2
VLA Archival Data

Source	Date	ID	ν (GHz)	Array	CLEAN Beam (″ × ″@°)	rms noise (μJy)
A11	1998 Jun 6	AB878	8.46	A/B	0.74 × 0.38@ 80.7	74
	2002 Oct 6	AL578	1.46	B/C	14.9 × 7.2 @ −71.7	80
A1664	1994 Nov 14	AE099	4.86	C	9.2 × 4.2 @ −24.7	100
A1835	1998 Apr 23	AT211	4.76	A	0.45 × 0.39 @ 30.0	47
ZWCL 348	1994 May 28	AK359	4.86	A/B	1.59 × 0.52 @ −72.2	66
ZWCL 3146	1994 Nov 14	AE099	4.86	C	4.61 × 4.42 @ 46.3	60
	1997 Jan 29	ACTST	4.86	A/B	1.52 × 0.47 @ −72.2	50
ZWCL 8193	1995 Aug 15	AM484	8.44	A	0.28 × 0.23 @ −83.1	180
	1997 Jun 27	AE110	4.86	C	4.29 × 3.75 @ −34.9	70
RXJ 2129+00	1998 Apr 12	AE117	8.46	A	0.26 × 0.24 @ −15.0	50
	2002 Jul 7	AH788	4.86	B	1.28 × 1.20 @ 1.7	35

Notes. The data for ZWCL 8193 have poor absolute flux density calibration.

continuum is patchy, as was true for A1795 and A2597 (O'Dea et al. 2004). As discussed in that work, the FUV continuum is likely associated with young stars in star clusters. The Lyα morphology contains both clumps and a more diffuse or filamentary component. The diffuse component is seen in Lyα but not in the FUV continuum, e.g., ZWCL 8193 (Figure 8). Diffuse or filamentary Lyα was also seen by O'Dea et al. (2004) in A1795 and A2597. The association between the Lyα and

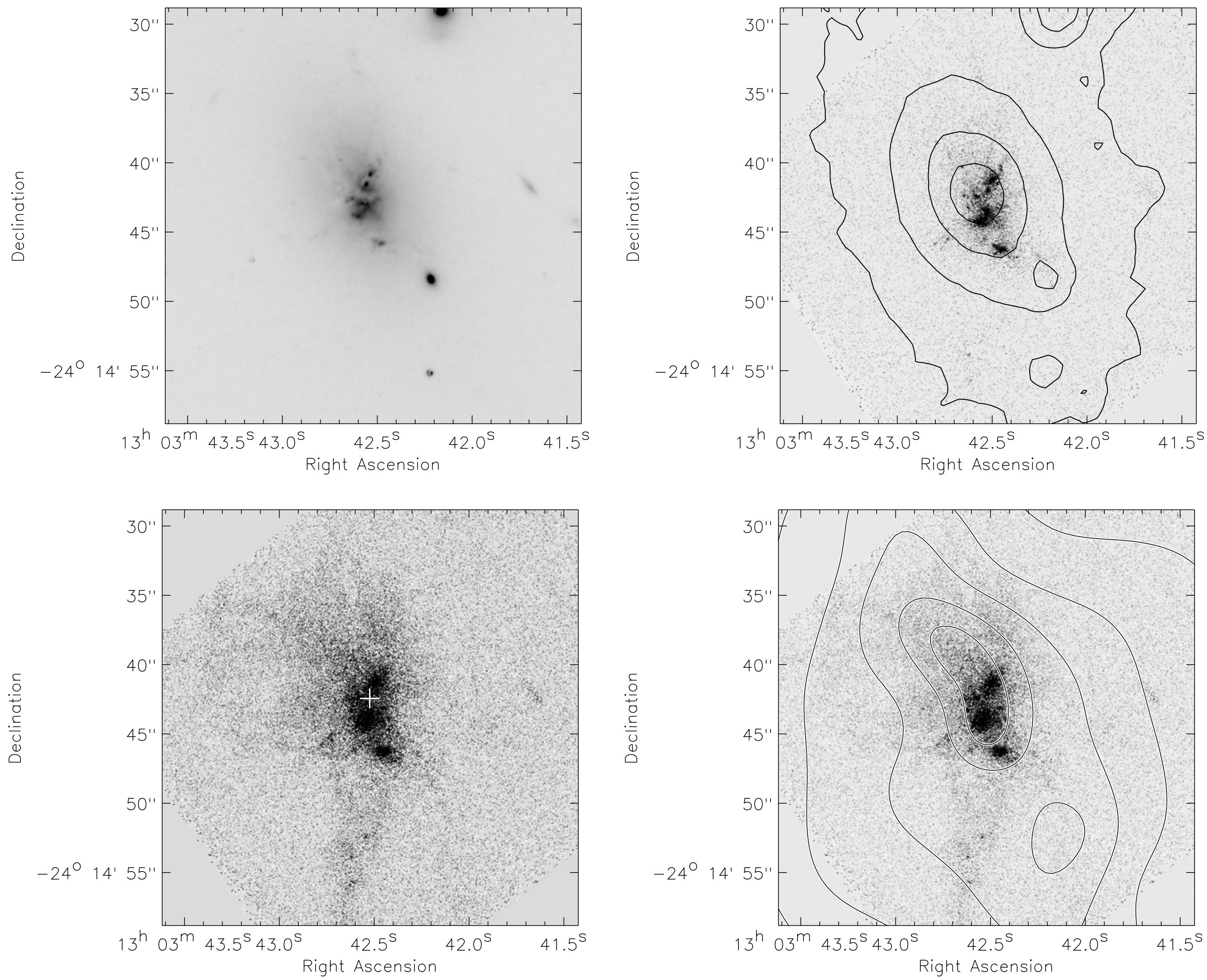

Figure 2. A1664. Upper left: *HST* WFPC2 *F606W* optical image of A1664. Note the dust lane. Upper right: *HST* SBC FUV continuum image with 3μm *Spitzer* IRAC band 1 contours overlaid. Contour separation is a factor of two in surface brightness. Lower left: continuum subtracted *HST* SBC Lyα image of A1664. The white cross marks the position of the unresolved VLA radio source (Table 4). Lower right: continuum subtracted Lyα image with *Chandra* X-ray contours. The peak of the Lyα emission is cospatial with that of the X-ray emission, although a second peak in the X-ray is detected to the southwest where there is a deficit of Lyα. At the redshift of A1664 ($z = 0.128$), 1″ corresponds ∼2.3 kpc.

FUV continuum implies that the FUV continuum contributes to the ionization of the Lyα emitting gas.

All of our BCGs display asymmetry in the FUV emission. In A11, the FUV continuum and Lyα emission are arranged in an extended clump cospatial with the visible nucleus, with a more diffuse component about 2″ west of the nucleus (also seen in the optical image). The main clump of emission is slightly offset from the center of the *Spitzer* IRAC 3 μm isophotes (see Figure 1). In A1664, three large clumps of FUV and Lyα trace the disturbed morphology of the host galaxy as observed in the optical. Additionally, there is a low surface brightness filament of Lyα emission extending ∼25 kpc to the south of the three bright clumps. This filament is not associated with any optical counterpart in the WFPC2 image or any FUV continuum emission. The 3 μm peak, cospatial with the galaxy's nucleus, is also cospatial with the dust lanes in the optical image (see Figure 2). A1835 has also been observed by Bildfell et al. (2008) who measure a size for the blue star-forming region of 19 ± 2 kpc, which is in good agreement with our measurement of ∼17 kpc for the size of the Lyα emission (Table 3) though McNamara et al. (2006) find blue colors on even larger scales. In A1835, the 3 μm contours are also not centered on the brightest regions seen in the FUV, Lyα, or visible band images (see Figure 3). For ZWCL 348, the visible and 3 μm emission peaks are nearly centered and the FUV emission peaks on the center of the galaxy. However, the visible band image shows that the galaxy is disturbed and the outer contours seen at 3 μm are not round (see Figure 4). The Lyα emission extends eastward from the nucleus much further than to the west. In ZWCL 3146, the FUV and Lyα emission are centered on the 3 μm contours (see Figure 5). For ZWCL 8193, there is a nuclear bulge in the optical and 3 μm images. However, FUV and Lyα emission are brighter north of the nucleus and have a spiral shape suggesting that a smaller galaxy has been recently disrupted in the outskirts of the BCG (see Figure 6). The host galaxy is an elliptical in a rich environment with several nearby dwarf satellites. The disturbed morphology of the host galaxy is suggestive of a recent or ongoing series of minor mergers. RXJ 2129+00 displays Lyα emission which

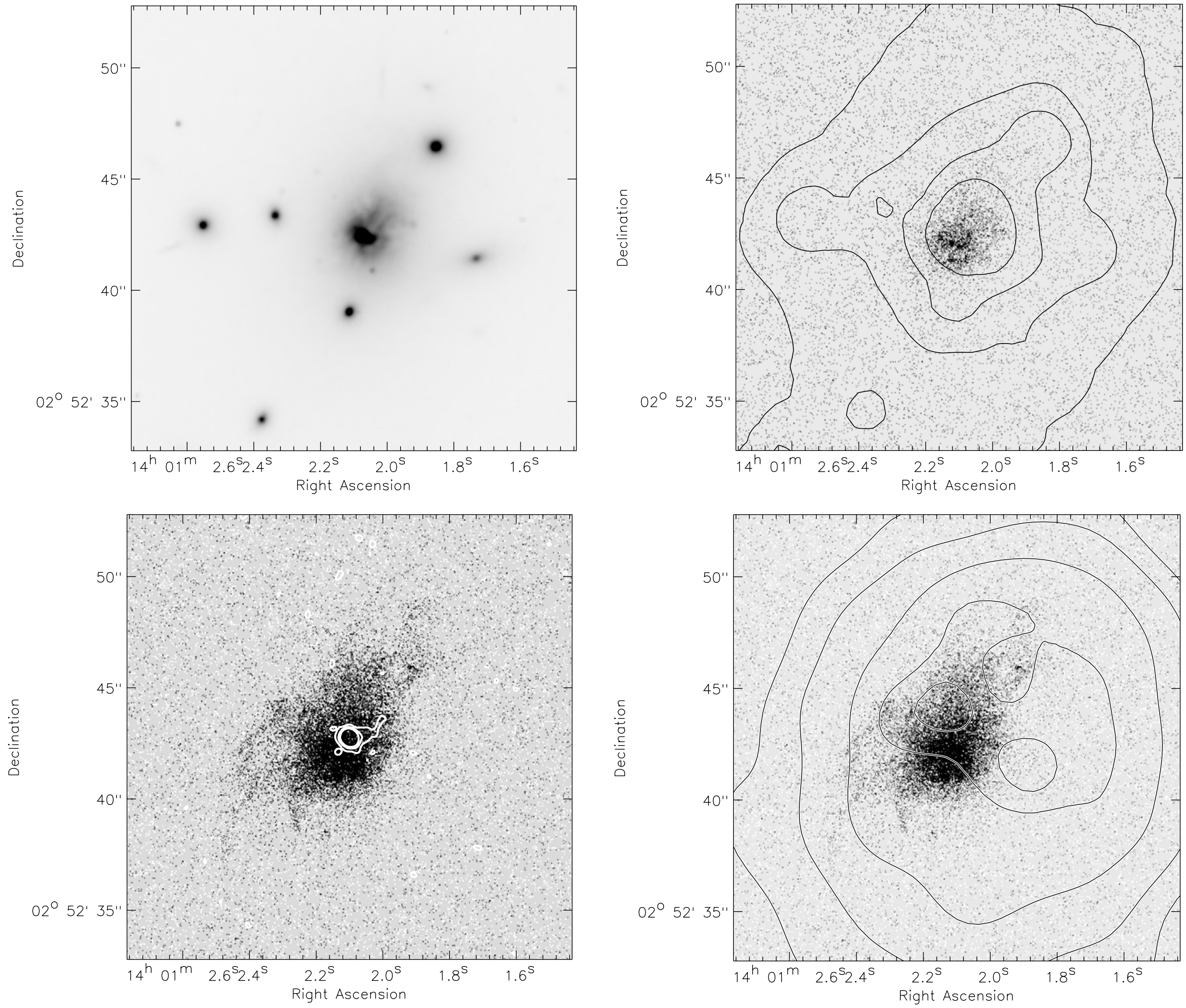

Figure 3. A1835. Upper left: *HST* WFPC2 *R*-band (*F702W*) image of A1835. Note the dust lane. Upper right: *HST* SBC FUV continuum image overlaid with *Spitzer* IRAC 3 μm contours. Lower left: continuum subtracted *HST* Lyα image of A1835 (gray scale) with 5 GHz VLA radio contours. There is no obvious relation between the Lyα and the radio jet. Lower right: continuum subtracted Lyα image with *Chandra* X-ray contours. As in A1664, the two peaks in X-ray emission are offset from the peak in the Lyα emission. At the redshift of A1835 ($z = 0.253$), 1″ corresponds to ~4 kpc.

extends on only the northeastern side of the galaxy. The offset between radio and Lyα peaks is small and so may be due to a registration error in the *HST* image (see Figure 7).

3.1.1. "Clumpiness" of FUV emission

We find that most of these BCGs display strong asymmetries or uneven distributions in their star formation as seen from the FUV continuum images (see Figure 9). For these galaxies, 1″ corresponds to 2–4 kpc (see Table 1) thus these asymmetries are on a scale of order 10–50 kpc. On smaller scales, the FUV morphology is generally more clumpy and filamentary than the associated Lyα component. For the purposes of this paper, we qualitatively define a "clump" as a compact region of emission a factor of ~2 brighter than the surrounding lower surface brightness diffuse component. A11, 1664, ZWCL 8193, and RXJ 2129+00 may be described as "clump dominated" in which the majority (>50%) of the FUV flux is associated with compact (<2 kpc) bright clumps. For example, the majority of FUV emission in A11 is associated with three bright clumps, the largest of which (the northern-most clump) extends ~0.6 kpc. The three bright clumps together contribute > ~ 60% of the total FUV flux from the source. The FUV morphology of RXJ 2129+00 is almost entirely associated with three small (~0.5 kpc) clumps and appears to lack a diffuse component. For A1835, ZWCL 348, and ZWCL 3146, the distinction between clumpy FUV emission and the diffuse component is less clear, and the flux seems to more gradually peak toward the center than, for example, ZWCL 8193. Note also that these galaxies are vastly more symmetric on >20 kpc scales than are the "clump-dominated" BCGs.

The high star formation rates of the galaxies studied here compared to others in the *ROSAT* BCG sample may be related to the large scale X-ray structure. We will discuss this in more detail later. Comparisons between Lyα and existing Hα images (not shown) suggest that there are large variations in emission line ratio. This can be explained either by patchy extinction or with shocks, affecting the intrinsic line ratios.

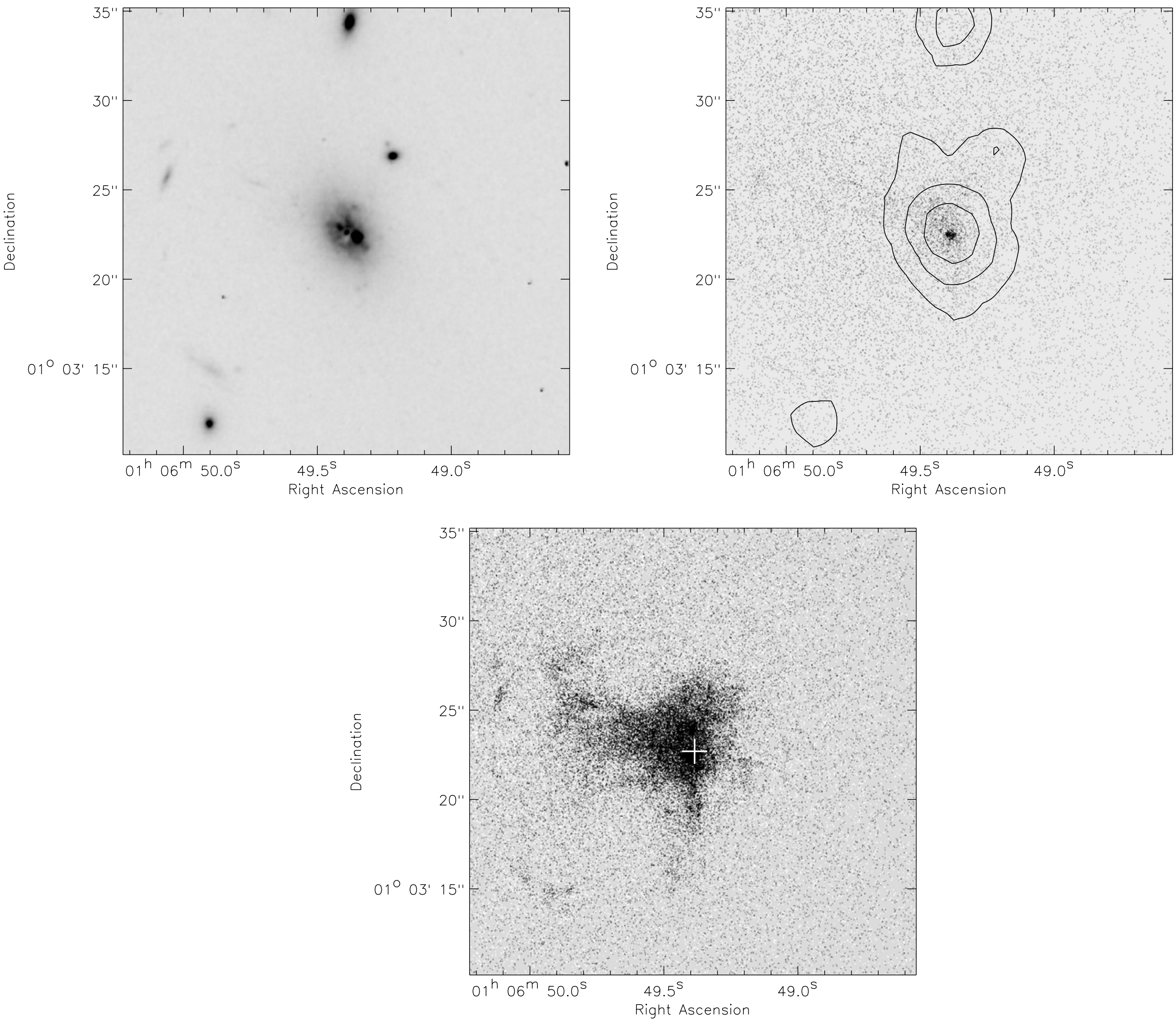

Figure 4. ZWCL 348. Upper left: optical *HST* WFPC2 *F606W* image of ZWCL 348. Note the dust lane. Upper right: FUV *HST* SBC continuum image overlaid with 3 μm contours. Bottom: continuum subtracted *HST* SBC Lyα image of ZWCL 348. The white cross marks the position of the unresolved VLA radio source (Table 4). At the redshift of ZWCL 348 ($z = 0.254$), 1″ corresponds to ~4 kpc.

Table 3
Lyα and FUV Continuum Properties

Source	Aperture Radius (″)	Cont. Sub. Lyα Flux (10^{-14} erg cm^{-2} s^{-1})	FUV Flux (10^{-14} erg cm^{-2} s^{-1})	L. A. S. Lyα arcsec (kpc)	L. A. S. FUV arcsec (kpc)	Morphology
A11	2.0	8.8 ± 0.3	18.9 ± 0.2	5.5 (14.5)	4.5 (11.7)	Lopsided, clumpy FUV, similar Lyα
A1664	3.0	7.7 ± 0.4	39.8 ± 0.2	18.0 (40.7)	12.2 (27.6)	Very clumpy and patchy, long filament to S
A1835	2.0	14.4 ± 0.3	22.9 ± 0.2	4.3 (17.0)	3.8 (14.8)	Symmetric "core," outer filaments
ZWCL 348	2.0	9.9 ± 0.3	11.8 ± 0.3	6.4 (24.8)	3.3 (12.9)	Clumpy, patchy, lopsided
ZWCL 3146	3.0	9.3 ± 0.3	17.7 ± 0.2	6.5 (28.1)	5.1 (22.0)	More symmetric, diffuse
ZWCL 8193	2.0	6.3 ± 0.4	42.8 ± 0.2	10.8 (31.8)	8.8 (25.8)	Clumpy, filamentary, lopsided
RXJ 2129+00	2.0	1.9 ± 0.7	2.1 ± 0.7	4.1 (15.3)	2.0 (7.4)	Lyα lopsided "shell," FUV faint

Notes. Fluxes were measured using aperture photometry and an aperture that covers the bulk of the emission visible in Figures 1–7. Errors are from count rate statistics. In general, the morphologies of the Lyα and FUV continuum emission were generally similar (unless otherwise noted), and the FUV emission typically spanned a slightly smaller linear extent than did the Lyα as it is less diffuse and extended. See the associated discussion in Section 3.

McNamara (1997) classified the morphology of star-forming regions in cooling core BCGs (studied using mainly ground-based optical observations) into four classes—point, disk, lobe, and amorphous. McNamara (1997) noted that the disks were very rare and that the amorphous morphologies are the most common. All of the seven BCGs studied here fall in the amorphous class. Why are disks so rare? We note that the star formation occurs over a large spatial scale (7–28 kpc). One

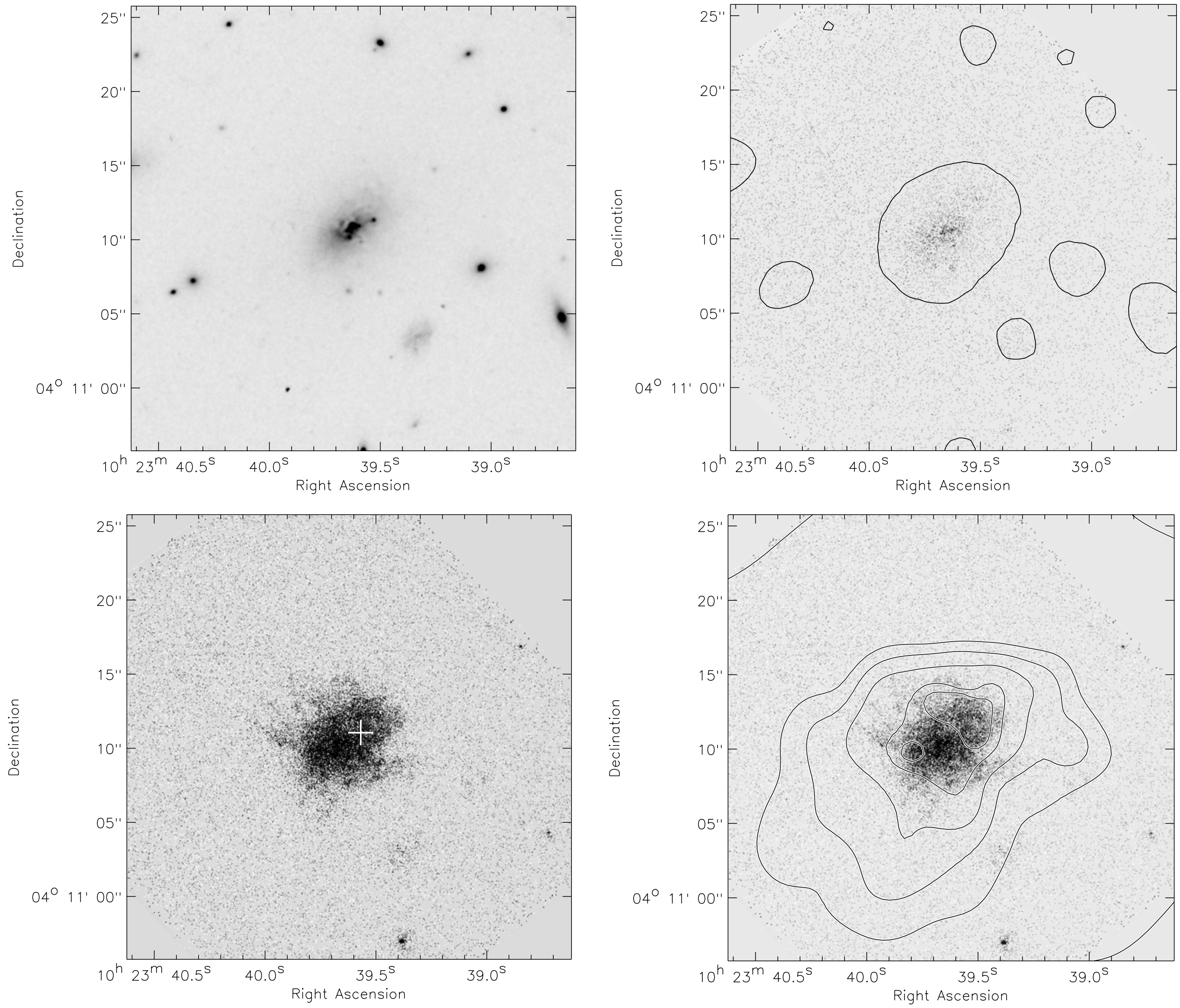

Figure 5. ZWCL 3146. Upper left: optical *HST* WFPC2 *F606W* image of ZWCL 3146. Upper right *HST* SBC FUV continuum image overlaid with 3 μm contours. Lower left: continuum subtracted *HST* SBC Lyα image of ZWCL 3146. The white cross marks the position of the unresolved VLA radio source (Table 4). Lower right: continuum subtracted Lyα image with X-ray contours. Note the asymmetry in the X-ray emission. At the redshift of ZWCL 3146 ($z = 0.290$), 1″ corresponds to ∼4.3 kpc.

possibility is that the stars form before the gas can collapse into a disk. In addition, studies of the kinematics of the optical emission-line nebulae in cool core BCGs find that the gas motions are mostly turbulent with very little organized rotation (e.g., Heckman et al. 1989; Baum et al. 1992; Wilman et al. 2006, 2009). Thus, the lack of star-forming disks may reflect the lack of systematic rotation in the star-forming gas.

3.1.2. Radio Emission

We detect a compact radio point source in all seven of the BCGs. In ZWCL 8193, the radio point source is 3 arcsec from the center of the BCG at the location of FUV-bright debris features and may be associated with a merging galaxy (Figure 6). The flux densities and spectral indices of the unresolved emission are given in Table 4. We find that the spectral indices of the point sources are steep. This suggests that the point sources are not flat spectrum parsec-scale-beamed jets but are possibly extended on at least tens of parsec scales. We also include Faint Images of the Radio Sky at Twenty-Centimeters (FIRST; Becker et al. 1995) flux densities and NVSS (Condon et al. 1998) flux densities, and powers in Table 4. The FIRST (∼5 arcsec) and NVSS (∼45 arcsec) flux densities are in good agreement indicating that there is very little additional flux density on scales between 5 and 45 arcsec. The mean value of the NVSS log powers for the seven BCGs is log $P_\nu = 24.33$; while A1795 is log $P_\nu = 24.87$ and A2597 is log $P_\nu = 25.42$. The radio powers for the seven BCGs are typical for our sample of 62 (Quillen et al. 2008; O'Dea et al. 2008).

We detect faint jets in RXJ 2129+00 and A1835. In RXJ 2129+00, the jet extends about 1 arcsec to the southeast of the core and has a flux density of 1.9 mJy at 8.46 GHz. The jet in A1835 has a total extent of about 1.5 arcsec and seems to start initially oriented to the west but then curves toward the northwest. The jet flux density is 2.3 mJy at 4.76 GHz. For these two we have overlaid radio contours on the images showing Lyα emission so the orientation of the radio emission can be seen.

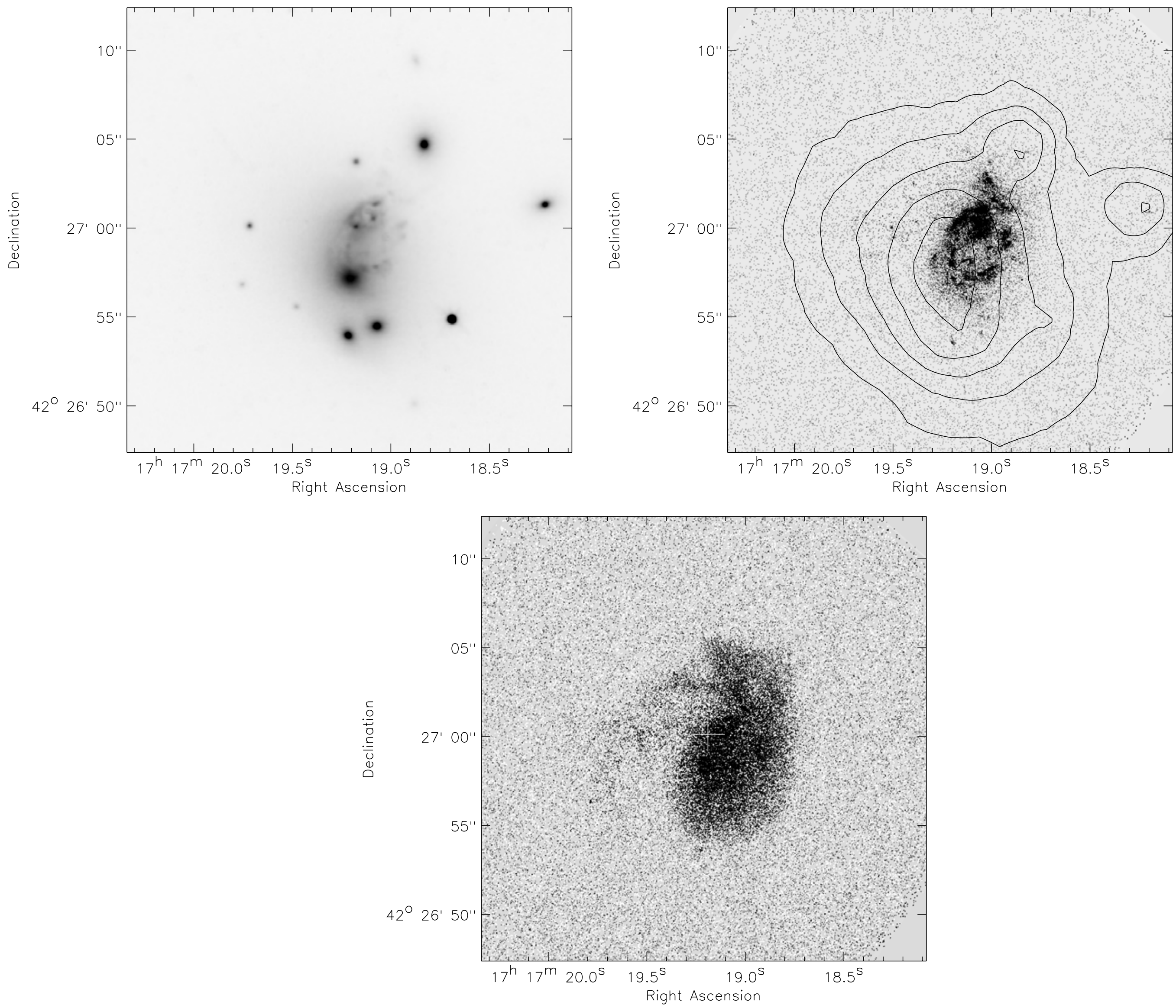

Figure 6. ZWCL 8193. Upper left: *HST* WFPC2 *F606W* image of ZWCL 8193. Note the dust lane. Uupper right: *HST* SBC FUV continuum image overlaid with 3μm contours. Bottom: continuum subtracted *HST* SBC Lyα image of ZWCL 8193. The Lyα filament has a spiral appearance. The white cross marks the position of the unresolved VLA radio source (Table 4). At the redshift of ZWCL 8193 ($z = 0.175$), 1$''$ corresponds to $\sim$3 kpc.

The radio jets are not clearly associated with Lyα emission or lying near emitting filaments in either galaxy as was true for the nearer galaxies A1795 and A2597 (O'Dea et al. 2004). We suggest that the more powerful radio sources in A1795 and 2597 are able to trigger star formation in their environments, while the weaker radio sources studied here are not. The lack of FUV emission aligned with the radio jet indicates that scattered AGN light (which would be aligned with the jet) does not contribute significantly.

Govoni et al. (2009) have found a faint, diffuse "mini-halo" around the BCG in A1835 which extends for several hundred kpc. The diffuse radio emission suggests that the AGN was much more active in the past and/or that A1835 has experienced a cluster merger (e.g., Murgia et al. 2009).

3.1.3. X-ray Morphology

Here, we discuss the X-ray structure and its relation to the BCG in the four sources for which we have X-ray imaging. For A1664, the outer 3 μm isophotes extend to the southwest where there is excess X-ray emission (see Figure 2). The asymmetric X-ray morphology was also noted by Kirkpatrick et al. (2009). A1835 also displays asymmetric X-ray structure (see Figure 3 and also Schmidt et al. 2001). Though the FUV and Lyα emission are centered on the 3 μm contours in ZWCL 3146, again the X-ray emission is lopsided, extending southeast of the nucleus (see Figure 5). RXJ 2129+00 also displays asymmetric X-ray emission contours extending to the southwest (see Figure 7).

We find that the four BCGs with X-ray imaging display asymmetries in the X-ray emission with A1664 previously noted by Kirkpatrick et al. (2009). We also see offsets between the BCG and the peak in the X-ray emission for all sources, ranging from 5 kpc for RXJ 2129+00 to 13 kpc for A1835, with a median offset of $\sim$10 kpc for all four.

In their study of 48 X-ray luminous galaxy clusters, Bildfell et al. (2008) observed similar significant offsets between the centroid of the brightest X-ray contour and that of the BCG. In that work the authors found a median offset of 14 kpc in

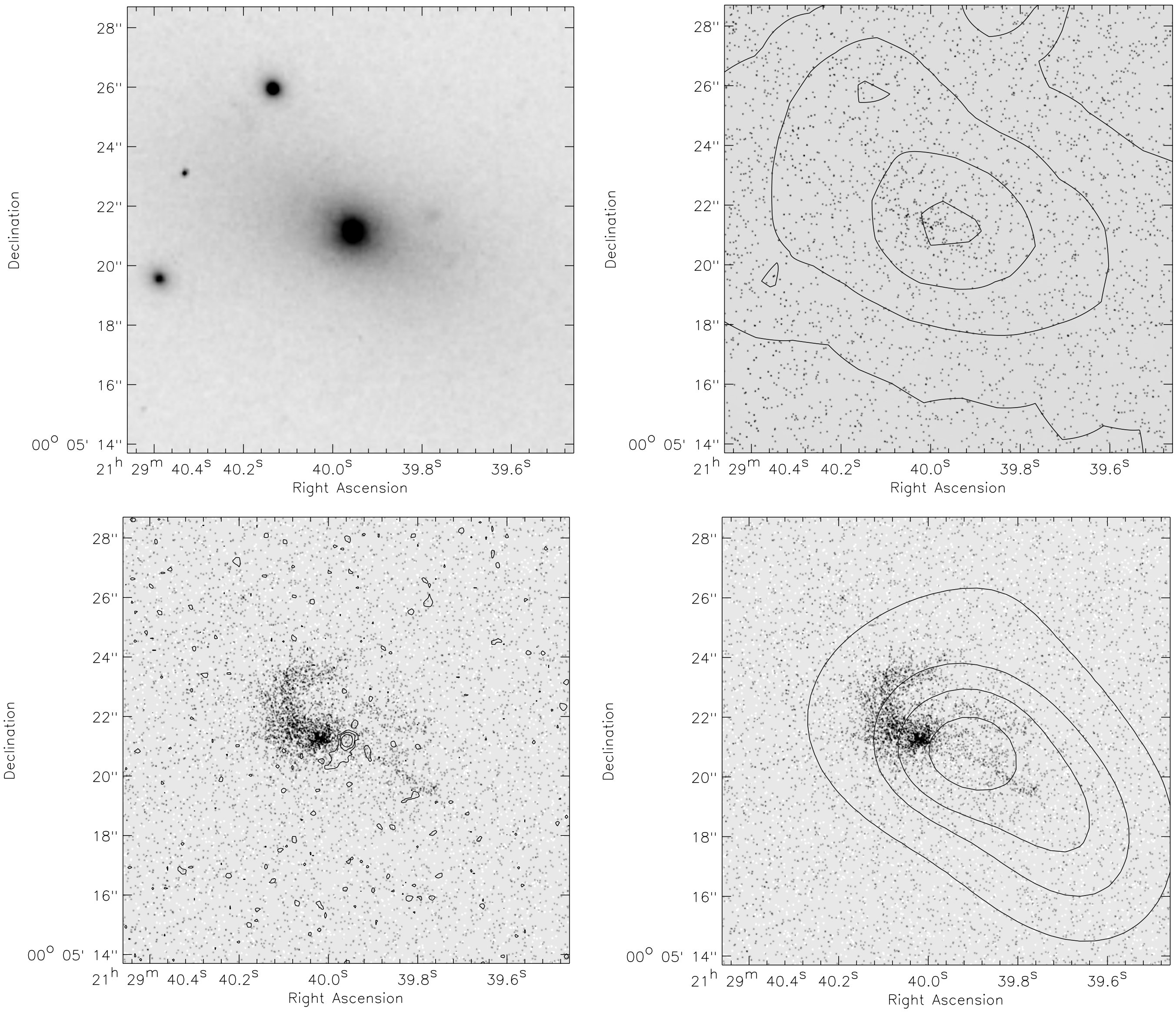

Figure 7. RXJ 2129+00. Upper left: optical *HST* WFPC2 *F606W* image of RXJ 2129+00. Upper right: *HST* SBC FUV continuum image overlaid with 3 μm contours. Lower left: continuum subtracted *HST* Lyα image of RXJ 2129+00 overlaid with 8 GHz VLA radio contours. Lower right: continuum subtracted Lyα image with X-ray contours. At the redshift of RXJ 2129+00 ($z = 0.235$), 1″ corresponds to ∼3.7 kpc.

their sample (and an average of 44 kpc). Sanderson et al. (2009) found that line-emitting BCGs all lie in clusters with an offset of <15 kpc in their sample of 65 X-ray selected clusters. Loubser et al. (2009), in their sample of 49 optically selected BCGs, found even larger offsets on average (median 27 kpc, mean 53 kpc). The offset of the BCG from the peak of the cluster X-ray emission is an indication of how close the cluster is to the dynamical equilibrium state, and decreases as the cluster evolves (Katayama et al. 2003). Our BCGs have offsets which are below the median for optically selected BCGs (Bildfell et al. 2008; Loubser et al. 2009) and are consistent with the trend for BCGs in cooling flows to have small offsets $\lesssim$10 kpc (Bildfell et al. 2008; Sanderson et al. 2009; but not seen by Loubser et al. 2009).

3.1.4. Comparison to CO and Hα observations

Emission from CO remained unresolved at a resolution of 6″ for A1835 and ZWCL 3146 (Edge & Frayer 2003). The *Spitzer* MIPS observations of these BCGs did not spatially resolve the 24 μm emission (Quillen et al. 2008; Egami et al. 2006). However, the IRAC observations of A1664 and ZWCL 8193 did resolve regions of very red color centered on the nucleus with a size of a few arc-seconds (Quillen et al. 2008). For comparison the PSF FWHM for IRAC camera is 1.″7 at 3 μm (IRAC band 1) and 2.″2 at 8 μm (IRAC band 4) and for MIPS is 7″ at 24 μm. Our *HST* FUV continuum images show that the star formation regions in these galaxies extend over a range of roughly 2–12 arcsec, corresponding to 7–28 kpc (Table 3). These sizes are consistent with the upper limits from the CO and *Spitzer* MIPS observations.

A1664 has been observed using integral field spectroscopy by Wilman et al. (2006) in the Hα line. The continuum subtracted Lyα emission image resembles the Hα image shown as Figure 2 by Wilman et al. (2006), with a bright spot about 2″ from the nucleus to the southwest. The bright spot we see just north of the nucleus does correspond to an Hα emission feature. However, the Ly emission is brighter northwest of the nucleus rather than northeast of the nucleus as is true in Hα. It is likely that a more

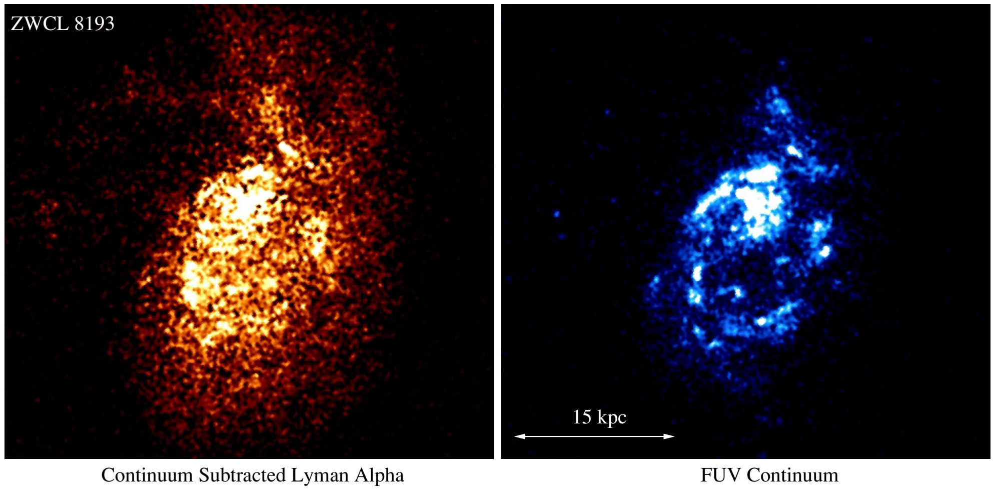

Figure 8. Comparison of continuum-subtracted Lyα and FUV continuum images for ZWCL 8193. In general, the Lyα is more diffuse, extended, and smoothly distributed than the underlying FUV continuum, which is more tightly arranged in clumpy and filamentary morphologies. The FUV continuum likely traces localized sites of star formation, which in turn photoionizes the smoother and more extended Lyα halos.

(A color version of this figure is available in the online journal.)

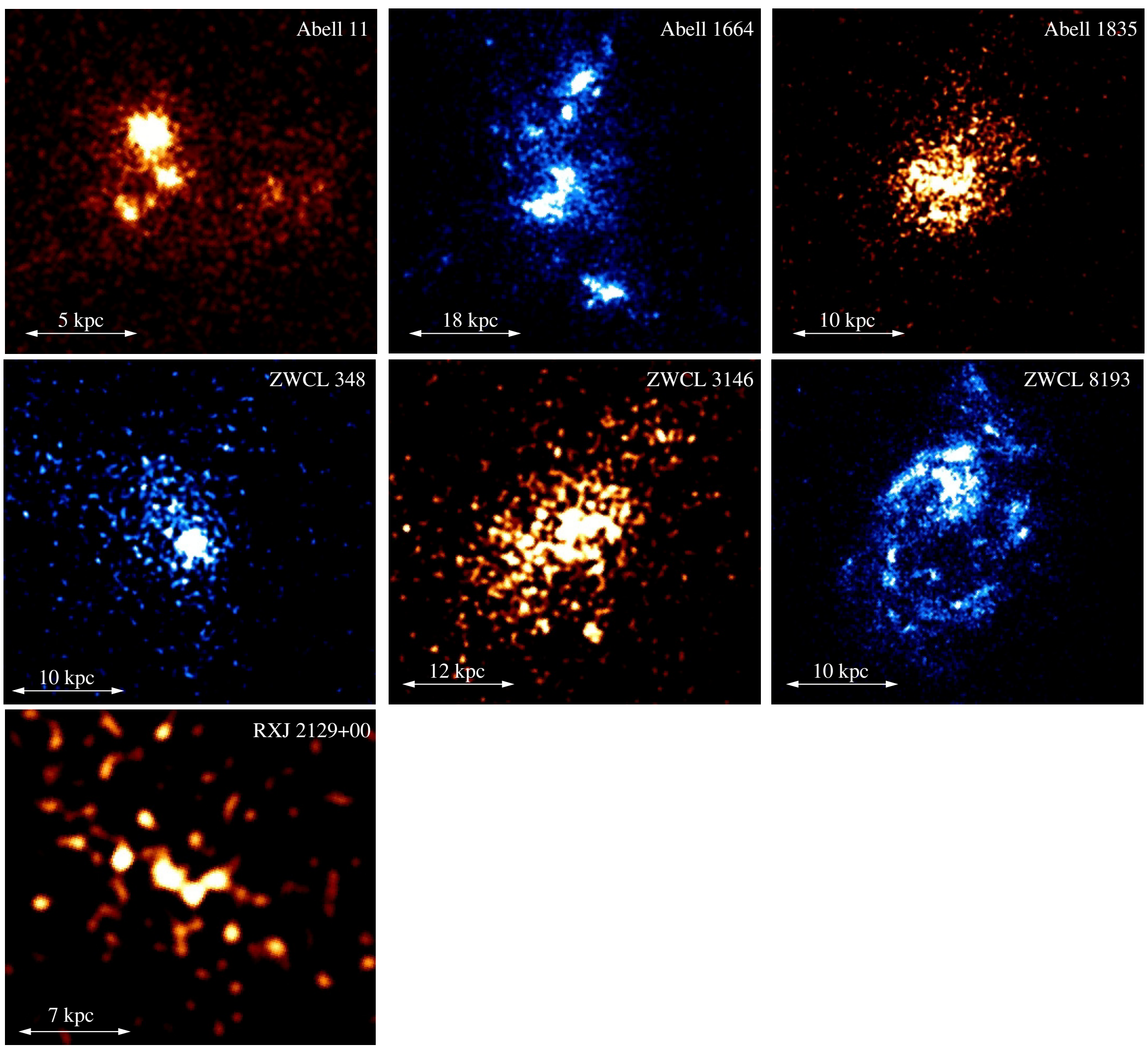

Figure 9. *HST*/ACS FUV images of the BCGs in our sample. Many exhibit clumpy and filamentary morphologies on <10 kpc scales and general asymmetries on >20 kpc scales. A11, 1664, ZWCL 8193, and RXJ 2129+00 may be described as "clump dominated" in which the majority (>50%) of the FUV flux is associated with compact bright clumps (as opposed to the lower surface brightness diffuse component). East is left, and north is up.

(A color version of this figure is available in the online journal.)

Table 4
Radio Properties of the Unresolved Emission

Source	R.A.	Decl.	ν (GHz)	S_ν (mJy)	α	FIRST S_ν (mJy)	NVSS S_ν (mJy)	NVSS log P_ν (W Hz^{-1})
A11	00:12:33.87	−16:28:07.7	8.46	21.3	−0.79	...	94.3	24.66
			1.46	85.6	...	...	...	...
A1664	13:03:42.52	−24:14:43.8	4.86	14.5	−0.74	...	36.4	24.09
A1835	14:01:02.10	+02:52:42.8	4.76	11.2	−0.84	31.3	39.3	24.75
ZWCL 348	01:06:49.39	+01 03 22.7	4.86	1.1	−0.93	3.5	∼1.4	23.31
ZWCL 3146	10:21:03.79	+04 26 23.4	4.86	0.6	−1.56	∼4.2	7.1	24.14
ZWCL 8193[a]	17:17:19.21	+42 26 59.9	8.44	64.8	−0.58	132.5	133.5	24.94
			4.86	89.2	...	...	...	...
RXJ 2129+00	21:29:39.96	+00:05:21.2	8.46	4.4	−0.86	24.3	25.4	24.48
			4.86	7.1	...	...	...	...

Notes. Columns 2 and 3: the right ascension and declination (J2000) of the unresolved radio source. Column 4: the frequency of observation. Column 5: the flux density of the point source in mJy. See Table 2 for details pertaining to these archival VLA observations. Column 6: the spectral index of the point source. We have used (1) the reprocessed archival data for A11, ZWCL 8193, and RXJ 2129+00, (2) the reprocessed archival data and the FIRST flux densities for A1835, ZWCL 348, and ZWCL 3146, and (3) the reprocessed archival data and the NVSS flux density for A1664. The spectral index is defined such that $S_\nu \propto \nu^\alpha$. Column 7: the integrated flux density at 1.4 GHz from VLA FIRST (Becker et al. 1995). Column 8: the integrated flux density from NVSS (Condon et al. 1998). Column 9: the power at 1400 MHz in the rest frame of the source using the NVSS flux density.
[a] The detected point source is 3 arcsec from the center of the BCG and is associated with apparent FUV bright debris features and thus may be associated with a merging galaxy.

detailed comparison will reveal a large variation in Lyα to Hα ratio suggesting either large variations in extinction or shock emission as photoionization models to predict a narrower range of intrinsic emission ratios (Ferland & Osterbrock 1985, 1986).

In A1835, the Hα and Lyα are both elongated along an NW–SE direction (Figure 3. We also see a dust lane along that orientation in the WFPC2 F702W image. The Hα integral field spectroscopy by Wilman et al. (2006) shows a velocity shear of $\sim$250 km s^{-1} along that direction which they suggest may be due to rotation.

Wilman et al. (2006) also observed ZWCL 8193 and detected Hα emission at the galaxy center and in two clumps about 3″ north of the galaxy (see their Figure 17). Their Hα emission more closely resembles our FUV continuum image, though the Hα emission is stronger near the galaxy than north of the galaxy and we see stronger continuum emission north of the galaxy than near the galaxy center. The Hα kinematics are complex. Our Lyα image shows diffuse emission over a region that is about twice the area than the Hα emission. The Lyα emission exhibits a tail curving to the east from the north and almost looks like a spiral galaxy.

3.2. *Estimated Star Formation Rates*

Pipino et al. (2009) used optical and NUV colors of BCGs to demonstrate that the UV light is produced by a young rather than old stellar population. We use the FUV continuum flux to estimate star formation rates in these galaxies. The continuum flux was first corrected for Galactic extinction. Extinction correction was done using Galactic extinction at the position of each BCG and the extinction law by Cardelli et al. (1989; as done in Table 5 by O'Dea et al. 2004 for A1795 and A2597). We then compared the count rate predicted for the observed filter by the STSDAS synthetic photometry package SYNPHOT for a spectrum produced by STARBURST99.[6] (Leitherer et al. 1999; Vazquez & Leitherer 2005).

The UV continuum estimated star formation rates are listed in Table 5. We compare the UV continuum estimated star formation with those based on the limited aperture Hα fluxes by Crawford et al. (1999) (using 1″.3 wide slit) or spectroscopic measurements from the Sloan Digital Sky Survey (SDSS) archive (using a 3″ diameter fiber) and those estimated from infrared observations with the *Spitzer Space Telescope* by Egami et al. (2006), Quillen et al. (2008), and O'Dea et al. (2008). Neither the UV continuum estimated nor Hα estimated star formation rates have been corrected for internal extinction. This table also lists molecular gas masses by Edge (2001) and Salome & Combes (2003).

Balmer decrements are available for most of the galaxies considered here and range from $\sim$3–5 (Crawford et al. 1999), see Table 5. Assuming an intrinsic Hα/Hβ theoretical line ratio of 2.86 ("case B" recombination; Osterbrock 1989), the observed Balmer decrement allows us to estimate the color excess associated with the internal extinction in the source, following the parameterization of Cardelli et al. (1989):

$$E\,(B-V)_{\mathrm{H}\alpha/\mathrm{H}\beta} = \frac{2.5\times\log\,(2.86/R_{\mathrm{obs}})}{k\,(\lambda_\alpha)-k\,(\lambda_\beta)}, \tag{1}$$

where $R_{\mathrm{obs}} = F\,(\mathrm{H}\alpha)\,/\,F\,(\mathrm{H}\beta)$ is the observed flux ratio, and the extinction curves at Hα and Hβ wavelengths are $k\,(\lambda_\alpha) \approx 2.63$ and $k\,(\lambda_\beta) \approx 3.71$, respectively, as given by Cardelli et al. (1989). One caveat is that if processes other than recombination (e.g., shocks, cosmic ray heating) contribute to Hα, the intrinsic Hα/Hβ ratio would be higher than the theoretical "case B" value and the estimated extinctions would be upper limits. With this possibility in mind, the upper-limit intrinsic optical extinction is $E(B-V)\sim 0.6$ for a Balmer decrement of 5, corresponding to an extinction in the FUV of $A_{\mathrm{FUV}} \sim 5.5$ and therefore a correction factor of 160 to the measured flux.

We note from Table 5 that IR star formation rates exceed those estimated in Hα and these exceed those estimated from the FUV continuum. This would be consistent with patchy but significant levels of extinction. The correction factor estimated for the UV photometry of 160 for a Balmer decrement of 5 is vastly higher than that required to make up the deficit of star formation rates estimated between the UV and (e.g.,) the IR. Large levels of extinction are also likely because of the high molecular gas content in these galaxies and the dust lanes

[6] http://www.stsci.edu/science/starburst99/

Table 5
Star Formation and Cluster Properties

Source	M(H_2) ($10^{10} M_\odot$ yr^{-1})	SFR$_{\rm IR}$ ($M_\odot$ yr^{-1})	SFR$_{\rm H\alpha}$ ($M_\odot$ yr^{-1})	SFR$_{\rm FUV}$ ($M_\odot$ yr^{-1})	Balmer Decl. (F [Hα/Hβ])	Central Entropy (KeV cm^2)	Central Cooling Time (Gyr)
A11	1.1	35	9.7	4.8	...	...	...
A1664	1.9	15	5.6	4.6	5.2	14.40	0.81
A1835	7.9	125	40.5	11.7	5	11.44	0.58
ZWCL 348		52	15.5	6.1	4.27	...	...
ZWCL 3146	7.0	67	47.1	12.4	3.7	11.42	0.59
ZWCL 8193	1.5	59	7.6	5.4	5.9	...	...
RXJ 2129+00		13	2.3	0.9	>2	21.14	0.82

Notes. Infrared estimated star formation rates are from O'Dea et al. (2008) except for A1835 and ZWCL 3146 which are by Egami et al. (2006). These star formation rates are estimated from the 8 and 24 μm fluxes (Quillen et al. 2008). Molecular gas mass estimates for A11, A1665, A1835, and ZWCL 3146 by Edge (2001), but corrected to a Hubble constant of 75 Mpc^{-1} km s^{-1}. The ZWCL 8193 molecular mass is by Salome & Combes (2003). Note ZWCL 3146 also contains about 10^{10} $M_\odot$ of warm molecular hydrogen (Egami et al. 2006). Star formation rates are estimated from the limited-aperture observations by Crawford et al. (1999) (long slit of width 1$''$.3) excepting for ZWCL 348 which used the Hα flux from the SDSS archive (and a 3$''$ diameter fiber). The central entropies and cooling times of the clusters are given by Cavagnolo et al. (2009). Neither the Hα nor UV based star formation rate estimates have been corrected for internal extinction.

seen in the optical images. Previous comparisons by Hu (1992) between Hα and Lyα flux suggested modest extinctions intrinsic to the cluster of order $E(B-V) \approx 0.09$–0.25. This was done assuming an unabsorbed Lyα/Hα ratio of 13 for photoionization and collision models (Ferland & Osterbrock 1986). However, the BCGs considered by Hu (1992) were not chosen via their Hα luminosity. As Hα luminosity is correlated with both molecular gas mass and infrared luminosity (O'Dea et al. 2008), it is perhaps not surprising that the sample considered here would have higher estimated internal extinctions than the same considered by Hu (1992).

In short, FUV estimated star formation rates range from $\sim$3 to $\sim$14 times lower than those estimated from the *Spitzer* observations. Balmer decrements and molecular gas observations suggest that internal extinction could be extremely high in some regions. The discrepancy between the estimated star formation rates and the internal extinction correction factor from the Balmer decrement suggests that internal extinction is patchy. As the infrared estimated star formation rate is least sensitive to extinction, it can be considered the most accurate, and suggests that about 90% of the FUV continuum has been absorbed. When taking patchy extinction into account, the discrepancy between star formation rates estimated at different wavelengths may be reconciled. Moreover, even when accounting for internal extinction, a one-to-one correspondence between star formation rates measured in the UV and IR are not necessarily expected, as the associated star formation indicators in those wavelength regimes may probe different aspects of the star-forming region (e.g., Johnson et al. 2007).

O'Dea et al. (2008) found that in gas-rich star-forming BCGs the nominal gas depletion time scale is about 1 Gyr. Since star formation is not highly efficient, it seems likely that 1 Gyr is an upper limit to the lifetime of the star formation. Pipino et al. (2009) suggest that the star formation in BCGs is relative recent with ages less than 200 Myr. Thus, a typical star formation rate of 50 $M_\odot$ yr^{-1} would result in a total mass of less than $10^{10} M_\odot$ which is a small fraction of the total stellar mass in a BCG (e.g., von der Linden et al. 2007) as also noted by, e.g., Pipino et al. (2009).

O'Dea et al. (2008) noticed a discrepancy between the infrared estimated star formation rates and the size of the star-forming regions. Here, we have confirmed that the star-forming regions are not large and remain under 30 kpc. This puts the galaxies somewhat off the Kennicutt relation (Kennicutt 1998) but (as shown by O'Dea et al. 2008 in their Figure 8) only by a modest factor of a few. While we confirm the discrepancy, we find that it is small enough that it could be explained by other systematic effects such as an overestimate of the H_2 mass. The CO to H_2 conversion factor is suspected to be uncertain by a factor of a few (e.g., Israel et al. 2006). Thus, there may be no significant discrepancy between the size of the star-forming regions as measured in the FUV and that predicted with the Kennicutt relation.

3.3. Is the Young Stellar Population Sufficient to Ionize the Nebula?

The fact that the Lyα morphology closely traces that of the underlying FUV continuum emission suggests that the latter provides at least a significant fraction of ionizing photons for the former, and that the nebula is ionized locally. Here, we explore this argument more quantitatively, in considering whether the observed FUV continuum is consistent with a sufficient number of hot stars required to ionize the nebula. This question can be addressed using simple arguments outlined by Zanstra (1931) and employed in similar contexts by (e.g., Baum & Heckman 1989; O'Dea et al. 2004). We assume a case B recombination scenario (Osterbrock 1989) in which the medium is optically thin to Balmer photons but optically thick to Lyman photons, and that in 10^4 K gas, $\sim$45% of all Balmer photons will emerge from the nebula as Hα photons. We further assume that all ionizing photons that are emitted by the stars are absorbed by the gas. This makes our estimate a rough lower limit, as in reality, a significant fraction of ionizing photons will escape, increasing the number of required stars.

Given these assumptions, the number of ionizing photons required to power the nebula is can be estimated via its observed Hα luminosity using the Zanstra (1931) method, which relates the emission-line luminosity to $Q_{\rm tot}$, the total number of photons with energies greater than 13.6 eV needed, per second, to ionize the nebula:

$$Q_{\rm tot} = \frac{2.2 L_{\rm H\alpha}}{h\nu_\alpha} \text{photons s}^{-1}, \tag{2}$$

where $L_{\rm H\alpha}$ is the total nebular Hα luminosity, h is Planck's constant, ν_α is the frequency of the Hα line, and 2.2 is the inverse of the 0.45 Balmer photon to Hα photon ratio assumed above.

Table 6
Can Hot Stars Ionize the Nebula?

Source	Hα Luminosity ($\mathrm{erg\ s^{-1}\ cm^{-2}}$)	Q_{required} (photons $\mathrm{s^{-1}}$)	SFR(Q_{required}) ($\dot{M}_{\odot}\ \mathrm{yr^{-1}}$)	$\left(\frac{\mathrm{SFR_{FUV}}}{\mathrm{SFR}[Q_{\mathrm{required}}]}\right)$
(1)	(2)	(3)	(4)	(5)
A11	...	...	...	...
A1664	6.38×10^{41}	4.64×10^{53}	2.12	2.17
A1835	1.68×10^{42}	1.22×10^{54}	5.58	2.09
ZWCL 348	1.95×10^{42}	1.41×10^{54}	6.47	0.94
ZWCL 3146	3.29×10^{42}	2.39×10^{54}	1.10	1.13
ZWCL 8193	2.79×10^{42}	2.03×10^{54}	9.29	0.58
RXJ 2129+00	3.33×10^{40}	2.42×10^{52}	1.11	8.1

Notes. Results of a photon-counting exercise designed to determine whether there are sufficient hot stars present (giving rise to the underlying FUV continuum) to ionize the emission-line nebula. We have used the Zanstra (1931) method relating the Hα emission-line luminosity with the number of ionizing photons required to give rise to that luminosity, assuming all ionizing photons are absorbed in 10^4 K gas obeying a case B recombination scenario. (1) Source name; (2) Hα luminosities in erg $\mathrm{s^{-1}\ cm^{-2}}$, from Crawford et al. (1999) excepting ZWCL 348, whose Hα luminosity is from the SDSS archive; (3) number of ionizing photons per second, required to ionize the nebula, as estimated using the Zanstra (1931) method described in Section 3.3; (4) star formation rate required to power the nebula, estimated by comparing Q_{required} with a STARBURST99 model calculating the number of photons with energies greater than 13.6 eV for a 10^7 yr old starburst assuming a continuous star formation rate of 1 $M_{\odot}\ \mathrm{yr^{-1}}$ and a initial mass function with an upper mass cutoff of 100 $M_{\odot}$ and slope $\alpha = 2.35$; (5) comparing the value calculated in Column 4 with the "observed" star formation rate as estimated by comparing our FUV photometry with the same STARBURST99 model. A ratio greater than 1 indicates that enough ionizing photons are present from the young stellar population to ionize the nebula. Obviously, there are significant uncertainties associated with these estimates. As such, this is meant only as an order-of-magnitude exercise. That the ratios are all of order unity indicates that the FUV emission due to the young stellar population is of sufficient strength to power the emission-line nebula.

For each galaxy in our sample (save A11, for which we do not have an Hα luminosity), we have calculated this value and scaled it in terms of a required star formation rate as predicted by the same STARBURST99 models used to calculate the star formation rates based on the FUV continuum. We present these results in Table 6. In every case, the ratio of the observed star formation rate to that required by the Zanstra method is of order unity, suggesting that the FUV continuum provides a significant fraction of ionizing photons for the nebula. Note that it is likely that stellar photoionization is not the only source of energy for cooling flow nebula (e.g., Voit & Donahue 1997). This result is consistent with the notion that the nebula is ionized locally by the young stars embedded within it, as supported by the similar morphologies of the Lyα emission and FUV continuum emission. O'Dea et al. (2004) undertook a similar exercise in their study of the cool core clusters A1795 and A2597, finding that there were enough hot stars present to within a factor of a few. They also estimated the degree to which a hidden quasar ionizing continuum would contribute ionizing photons, finding that a modest AGN luminosity could contribute ∼10% of what was required.

4. DISCUSSION AND SUMMARY

In this paper, we have presented high-angular resolution images in FUV continuum and Lyα of 7 BCGs selected on the basis of IR emission which suggested the presence of significant star formation. We confirm that the BCGs are actively forming stars. This confirms that the IR excess seen in these BCGs is indeed associated with star formation. Our observations are consistent with a scenario in which gas which cools from the ICM fuels the star formation (O'Dea et al. 2008; Bildfell et al. 2008; Loubser et al. 2009; Pipino et al. 2009). The FUV continuum emission extends over a region ∼7–28 kpc (largest linear size) and even larger in Lyα. Both continuum and line emission contain clumps and filaments, but the Lyα emission also contains a diffuse component.

Star formation rates estimated from the FUV continuum range from about 3–14 times lower than those estimated from the infrared. However, both the Balmer decrement in the central arcsec, the presence of dust lanes seen in the optical images, and the detection of CO in these galaxies suggests that there are regions of dense gas and high extinction within the central 10–30 kpc. Thus, the lower star formation rates estimated in the FUV are consistent with the expected internal extinction.

We find that the young stellar population required by the FUV observations would produce a significant fraction of the ionizing photons required to power the emission-line nebula.

We find unresolved radio emission in each of the seven BCGs. In addition, A1835 and RXJ 2129+00 also exhibit weak kpc scale jets. The unresolved radio emission in ZWCL 8193 is offset from the center of the BCG by 3 arcsec and may be associated with a merging galaxy. These BCGs tend to have fairly compact (<1 kpc), weak, steep spectrum radio structures. The hypothesis that the radio source is confined to the sub-kpc scale by dense gas (as originally suggested for GPS and CSS sources, e.g., Wilkinson et al. 1984; van Breugel et al. 1984; O'Dea et al. 1991; O'Dea 1998) could be tested via VLBI observations. On the other hand, the radio properties could be explained if nuclear fueling has been reduced by a previous AGN activity cycle and we are now seeing the galaxies following a period of relative AGN quiescence. It is tempting to also account for the high star formation rate with a period of low feedback. Rapid cooling in the IGM fueling the current high star formation may be due to a previous reduction in energy deposited into the IGM. Kirkpatrick et al. (2009) find that cooling rates could be high enough to fuel the star formation in A1664. Similar cooling rates have been estimated for most of the other galaxies in our sample (O'Dea et al. 2008).

We note that there is FUV continuum and Lyα emission in A1795 and A2597 which is closely associated with the radio sources—suggesting a contribution from jet induced star formation (O'Dea et al. 2004). However, the radio jets in A1835 and RXJ 2129+00 show no relationship with the FUV emission. While both A1795 and A2597 host star formation, it is at a lower level than estimated for the seven of our sample. In addition, the seven BCGs studied here are generally have less powerful radio sources than those in A1795 and A2597. The combination of higher SFR and lower radio power in our BCGs suggests that the radio sources have a smaller relative impact on the triggering and/or properties of the star formation and associated emission-line nebulae. Further, the lack of FUV emission aligned with the radio jets indicates that the contribution from scattered AGN light is small.

We have also noted that most of our galaxies exhibit asymmetries in their distribution of star formation and four of them show lopsided X-ray contours. Feedback from an AGN (jets and bubbles) would not be expected to push the X-ray emitting gas off-center. However, disturbances in the IGM could lead to higher cooling rates in the gas as the cluster relaxes and slowly evolves to equilibrium (e.g., Russell et al. 2010).

We thank the referee for a prompt and constructive report. This work is based on observations made with the NASA/ESA *Hubble Space Telescope*, obtained at the Space Telescope Science Institute, which is operated by the Association of Universities for Research in Astronomy, Inc., under NASA contract 5-26555. Support for *HST* program 11230 was provided by NASA through a grant from the Space Telescope Science Institute, which is operated by the Association of Universities for Research in Astronomy, Inc., under NASA contract NAS 5-26555. This research made use of (1) the NASA/IPAC Extragalactic Database (NED) which is operated by the Jet Propulsion Laboratory, California Institute of Technology, under contract with the National Aeronautics and Space Administration; and (2) NASA's Astrophysics Data System Abstract Service. The National Radio Astronomy Observatory is a facility of the National Science Foundation operated under cooperative agreement by Associated Universities, Inc. K.P.O. was supported by an NSF REU program at the University of Rochester.

REFERENCES

Allen, S. W. 1995, MNRAS, 276, 947
Baum, S. A., & Heckman, T. 1989, ApJ, 336, 681
Baum, S. A., Heckman, T. M., & van Breugel, W. 1992, ApJ, 389, 208
Becker, R. H., White, R. L., & Helfand, D. J. 1995, ApJ, 450, 559
Bildfell, C., Hoekstra, H., Babul, A., & Mahdavi, A. 2008, MNRAS, 389, 1637
Binette, L., Wang, J., Villar-Martin, M., Martin, P. G., & Magris, G. G. 1993, ApJ, 414, 535
Cardelli, J. A., Clayton, G. C., & Mathis, J. S. 1989, ApJ, 345, 245
Cardiel, N., Gorgas, J., & Aragon-Salamanca, A. 1998, Ap&SS, 263, 83
Cavagnolo, K. W., Donahue, M., Voit, G. M., & Sun, M. 2008, ApJ, 683, L107
Cavagnolo, K. W., Donahue, M., Voit, G. M., & Sun, M. 2009, ApJS, 182, 12
Clampin, M., et al. 2004, in Scientific Detectors for Astronomy, The Beginning of a New Era, ed. P. Amico, J. W. Beletic, & J. E. Beletic (Dordrecht: Kluwer), 555
Condon, J. J., Cotton, W. D., Greisen, E. W., Yin, Q. F., Perley, R. A., Taylor, G. B., & Broderick, J. J. 1998, AJ, 115, 1693
Cowie, L. L., & Binney, J. 1977, ApJ, 215, 723
Crawford, C. S., Allen, S. W., Ebeling, H., Edge, A. C., & Fabian, A. C. 1999, MNRAS, 306, 857
Crawford, C. S., & Fabian, A. C. 1993, MNRAS, 265, 431
Ebeling, H., Edge, A. C., Böhringer, H., Allen, S. W., Crawford, C. S., Fabian, A. C., Voges, W., & Huchra, J. P. 1998, MNRAS, 301, 881
Ebeling, H., White, D. A., & Rangarajan, F. V. N. 2006, MNRAS, 368, 65
Edge, A. C. 2001, MNRAS, 328, 762
Edge, A. C., & Frayer, D. T. 2003, ApJ, 594, L13
Edge, A. C., Stewart, G. C., & Fabian, A. C. 1992, MNRAS, 258, 177
Egami, E., Rieke, G. H., Fadda, D., & Hines, D. C. 2006, ApJ, 652, L21
Egami, E., et al. 2006, ApJ, 647, 922
Fabian, A. C., & Nulsen, P. E. J. 1977, MNRAS, 180, 479
Ferland, G. J., & Osterbrock, D. E. 1985, ApJ, 289, 105
Ferland, G. J., & Osterbrock, D. E. 1986, ApJ, 300, 658
Govoni, F., Murgia, M., Markevitch, M., Feretti, L., Giovannini, G., Taylor, G. B., & Carretti, E. 2009, A&A, 499, 371
Hansen, L., Jorgensen, H. E., & Norgaard-Nielsen, H. U. 1995, A&A, 297, 13
Heckman, T. M., Baum, S. A., van Breugel, W. J. M., & McCarthy, P. 1989, ApJ, 338, 48
Hicks, A. K., & Mushotzky, R. 2005, ApJ, 635, L9
Holtzman, J. A., et al. 1996, AJ, 112, 416
Hu, E. M. 1992, ApJ, 391, 608
Hutchings, J. B., & Balogh, M. L. 2000, AJ, 119, 1123
Israel, F. P., Tilanus, R. P. J., & Baas, F. 2006, A&A, 445, 907
Johnson, B. D., et al. 2007, ApJS, 173, 392
Johnstone, R. M., Fabian, A. C., & Nulsen, P. E. J. 1987, MNRAS, 224, 75
Katayama, H., Hayashida, K., Takahara, F., & Fukita, Y. 2003, ApJ, 585, 687
Kennicutt, R. C. 1998, ApJ, 498, 541
Kirkpatrick, C. C., et al. 2009, ApJ, 697, 867
Leitherer, C., et al. 1999, ApJS, 123, 3
Loubser, S. I., Sanchez-Blazquez, P., Sansom, A. E., & Soechting, I. K. 2009, MNRAS, 398, 133
McNamara, B. R. 1997, in ASP Conf. Ser. 115, Galactic Cluster Cooling Flows, ed. N. Soker (San Francisco, CA: ASP), 109
McNamara, B. R. 2004, in The Riddle of Cooling Flows in Galaxies and Clusters of Galaxies, ed. T. Reiprich, J. Kempner, & N. Soker (Charlottesville, VA: Univ. Virginia) 177
McNamara, B. R., & O'Connell, R. W. 1989, AJ, 98, 2018
McNamara, B. R., & O'Connell, R. W. 1993, AJ, 105, 417
McNamara, B. R., Rafferty, D. A., Birzan, L., Steiner, J., Wise, M. W., Nulsen, P. E. J., Carilli, C. L., Ryan, R., & Sharma, M. 2006, ApJ, 648, 164
McNamara, B. R., Wise, M. W., & Murray, S. S. 2004, ApJ, 601, 173
Mittaz, J. P. D., et al. 2001, A&A, 365, L93
Murgia, M., Govoni, F., Markevitch, M., Feretti, L., Giovannini, G., Taylor, G. B., & Carretti, E. 2009, A&A, 499, 679
O'Dea, C. P. 1998, PASP, 110, 493
O'Dea, C. P., Baum, S. A., Mack, J., Koekemoer, A. M., & Laor, A. 2004, ApJ, 612, 131
O'Dea, C. P., Baum, S. A., & Stanghellini, C. 1991, ApJ, 380, 66
O'Dea, C. P., et al. 2008, ApJ, 681, 1035
Oegerle, W. R., et al. 2001, ApJ, 560, 187
Osterbrock, D. E. 1989, Astrophysics of Gaseous Nebulae and Active Galactic Nuclei (Mill Valley, CA: Univ. Science Books)
Pipino, A., Kaviraj, S., Bildfell, C., Babul, A., Hoekstra, H., & Silk, J. 2009, MNRAS, 395, 462
Quillen, A. C., et al. 2008, ApJS, 176, 39
Rafferty, D. A., McNamara, B. R., & Nulsen, P. E. J. 2008, ApJ, 687, 899
Rafferty, D. A., McNamara, B. R., Nulsen, P. E. J., & Wise, M. W. 2006, ApJ, 652, 216
Romanishin, W. 1987, ApJ, 323, L113
Russell, H. R., Sanders, J. S., Fabian, A. C., Baum, S. A., Donahue, M., Edge, A. C., McNamara, B. R., & O'Dea, C. P. 2010, MNRAS, in press
Salome, P., & Combes, F. 2003, A&A, 414, 657
Sanderson, A. J. R., Edge, A. C., & Smith, G. P. 2009, MNRAS, 398, 1698
Schmidt, R. W., Allen, S. W., & Fabian, A. C. 2001, MNRAS, 327, 1057
Smith, E. P., Bohlin, R. C., Bothum, G. D., O'Connell, R. W., Roberts, M. S., Neff, S. G., Smith, A. M., & Stecher, T. P. 1997, ApJ, 478, 516
van Breugel, W., Heckman, T., & Miley, G. 1984, ApJ, 276, 79
Vazquez, G. A., & Leitherer, C. 2005, ApJ, 621, 695
Voit, G. M., Cavagnolo, K. W., Donahue, M., Rafferty, D. A., McNamara, B. R., & Nulsen, P. E. J. 2008, ApJ, 681, L5
Voit, G. M., & Donahue, M. 1997, ApJ, 486, 242
von der Linden, A., Best, P. N., Kauffmann, G., & White, S. D. M. 2007, MNRAS, 379, 867
Wilkinson, P. N., Booth, R. S., Cornwell, T. J., & Clark, R. R. 1984, Nature, 308, 619
Wilman, R. J., Edge, A. C., & Swinbank, A. M. 2006, MNRAS, 371, 93
Wilman, R. J., Edge, A. C., & Swinbank, A. M. 2009, MNRAS, 395, 1355
Zanstra, H. 1931, Publ. Dom. Astrophys. Obs., 4, 209